Linear and Nonlinear Diagnostic Models of Stationary Eddies in the Upper Troposphere during Northern Summer

IN-SIK KANG*

Geophysical Fluid Dynamics Program, Princeton University, Princeton, NJ 08542

ISAAC M. HELD

Geophysical Fluid Dynamics Laboratory/NOAA, Princeton University, Princeton, NJ 08542

(Manuscript received 25 January 1986, in final form 11 June 1986)

ABSTRACT

The upper tropospheric circulation during northern summer produced by a general circulation model (GCM) is studied using linear and nonlinear barotropic models and by analyzing a streamfunction budget. The model experiments and the budget calculations both show a simple Sverdrup balance to be a useful first approximation for the largest scales during this season. In this Sverdrup balance, the advection of planetary vorticity by the divergent component of the flow is found to be significant, particularly in the Southern Hemisphere tropics.

Nonlinear barotropic models improve the simulation of regional structures. The correct position of the Tibetan high is explained by Sverdrup balance, but its amplitude and structure are reasonably well simulated only with the nonlinear models. With climatological forcing, the time-averaged solutions of the nonlinear model are insensitive to the strength of the damping included in the model. The difference between the GCM's climatology and the GCM's flow in a particular summer is more difficult to model because of the large contribution of anomalous transients to the maintenance of the flow. However, strongly damped models produce simulations that bear some resemblance to the anomalous flow, at least in the tropics.

To estimate the potential importance of vertical transport of momentum during moist convection, a damping proportional to the precipitation rate in the GCM is added in the nonlinear model. The estimated damping time scale for the eddy streamfunction is ~5 days in the northern tropics, but the changes in the predicted stationary eddy streamfunction are modest.

1. Introduction

In the tropics, the horizontal structure of the climatological upper-tropospheric divergence is closely controlled by the horizontal structure of the latent heating. In regions where convection is concentrated, latent heating is balanced to an excellent approximation by adiabatic cooling due to upward motion. The dynamically induced heating in regions of compensating subsidence is balanced by radiative cooling (to the extent that this subsidence occurs in the deep tropics where horizontal temperature advection is negligible). The vortex tube stretching and compression associated with this vertical motion field drive the upper tropospheric flow. In light of these balances, the following questions form a natural sequence:

- How is the climatological tropical latent-heating distribution determined?
- How is the distribution of upper tropospheric divergence determined by the latent heating? (Or, what is essentially equivalent, how can one model the planetary-scale subsidence given the latent heating?)
- How is the upper tropospheric streamfunction determined by the divergence?

We address only the third question in this paper. Admittedly, we would prefer to address the second as well, as do the linear models of Gill (1980), Webster (1981) and Kang (1984), and the nonlinear axially symmetric model of Schneider (1977), for example. However, we feel the simplification afforded by specifying the divergence is very useful as one attempts to simulate realistic flows and to explore such issues as the importance of nonlinearity and transient mixing. The relevant model becomes the barotropic vorticity equation at an upper tropospheric level forced by a specified divergence; one can ignore the dynamics at other levels.

Fixing the mean divergence and predicting the mean streamfunction at some level in the atmosphere is not always a very useful exercise. For example, if the mean flow is dominated by free vertically propagating waves, or external Rossby waves propagating horizontally through a vertically sheared flow (e.g., Held et al., 1985), then the divergence and the vorticity are both essential components of the same wave and fixing one

* Present affiliation: Department of Atmospheric Sciences, Seoul National University, Seoul 151 Korea.

while predicting the other does not help in isolating the wave sources and sinks. It is the fact that the mean divergence is so tightly constrained by the latent heating distribution that makes such a calculation dynamically meaningful in the tropics.

In this paper we focus on the stationary eddies in Northern Hemisphere summer. There is an important distinction between summer and winter in the tropics, in that the upper tropospheric easterlies are more extensive in Northern Hemisphere summer, ultimately due to the fact that convective heating moves farthest from the equator during this season. As a result, stationary Rossby waves are excluded from a larger region and the flow has more of the character of local responses to localized forcing. We suspect that the tropics in Northern Hemisphere summer are somewhat easier to model for this reason.

The simplest conceivable model of the upper-tropospheric stationary eddies is a Sverdrup balance, $\beta v = -fD$, where D is the prescribed divergence. Following Holton and Colton (1972), it has often been argued that this balance fails in the Northern Hemisphere summer, in particular with regard to the position of the most prominent feature of the summertime climatology, the Tibetan anticyclone, and that a likely reason is the damping effect on the upper tropospheric flow of small-scale vertical mixing of momentum during moist convection. The importance of this "cumulus friction" for the planetary-scale flow remains controversial. Chang (1977), Schneider and Lindzen (1977) and Yanai et al. (1982) argue for its importance. On the other hand, Sardeshmukh and Held (1984) and Sardeshmukh and Hoskins (1985) emphasize the importance of nonlinearity in the vorticity equation and argue indirectly that cumulus friction is of minor importance. Sardeshmukh and Held (1984) examines the flow generated by a GCM in which there is no momentum transport by the convective parameterization; the flow has a reasonable large-scale structure, and the local vorticity budget is found to be strongly nonlinear, with stretching balanced primarily by advection of relative vorticity. Sardeshmukh and Hoskins (1985) is a study of the vorticity budget using observations (for the tropics in Northern Hemisphere winter) analyzed at the European Centre for Medium Range Weather Forecasting. Again the impression gained is that nonlinearity is of more concern than the residual small-scale mixing. The claim here is not that the estimates of the momentum transport during cumulus convection, particularly the careful analyses of the GATE data exemplified by Sui and Yanai (1986), are in error, but that this mixing is of secondary importance for the planetary-scale flow.

Aside from the question of small-scale vertical mixing, there is the question of the importance of quasi-horizontal mixing by large-scale eddies. How important is such mixing for the climatological tropical flow? Can some of the eddies responsible for this mixing be modeled in a barotropic framework, as the work of Simmons et al. (1983) suggests may be possible? This is especially problematic with regard to the zonally averaged flow. As one moves into the subtropics, the Coriolis force acting on the zonal mean meridional circulation, $f\bar{v}$, is primarily balanced by transient eddy vorticity fluxes due to eddies generated baroclinically in midlatitudes. There is no reason to expect comparable fluxes to be generated in a barotropic model, so there is nothing preventing $\bar{u}$ from drifting toward unrealistic values in such a model. The problem is particularly acute in a model in which the divergence is specified, for then one has also specified $\bar{v}$. Therefore, we concentrate on the maintenance of the deviations from zonal symmetry, the stationary eddies, and not the maintenance of the zonally averaged flow.

We begin in section 2 by analyzing the climatological 200 mb flow produced by a general circulation model in Northern Hemisphere summer. Time-mean vorticity budgets in GCMs (and presumably in nature as well) are noisy and difficult to interpret (see Sardeshmukh and Held, 1984). We consider a streamfunction budget instead, with the hope that the resulting broader scale structures, obtained by operating with the inverse of the Laplacian on all terms in the vorticity equation, will be more useful for comparison with the balances produced by idealized models. We also describe how the circulation and the streamfunction budget in an individual summer simulated by the GCM differ from the GCM's climatology.

In sections 3 and 4 we examine several linear and nonlinear barotropic models with which we try to simulate the GCM's stationary eddy streamfunction by specifying the divergence field and the zonally averaged zonal flow. In these modeling studies and in the analysis of the GCM's streamfunction budget, we are particularly concerned with evaluating the usefulness of Sverdrup balance as a zero-order approximation to the flow, the relative importance of stationary nonlinearity and transients, and the importance of advection of vorticity by the divergent flow.

There is no mixing of momentum by the cumulus parameterization in the GCM we analyze, so the possible importance of cumulus friction is not addressed in our attempts to analyze the GCM's flow with barotropic models. However, we describe some additional calculations in section 5 in which we add a momentum damping with strength proportional to the GCM's local precipitation rate so as to gain some feeling for the manner in which such mixing would alter the planetary-scale flow.

2. The GCM and its summertime streamfunction budget

The general circulation model analyzed is a spectral model developed at GFDL. Its relatively low-resolution, rhomboidal truncation at wavenumber 15 makes

extended integrations possible but also undoubtedly introduces some distortion into the tropical flow simulation. In particular, one cannot generate a sharp ITCZ at this resolution. It is also known that the zonally averaged Hadley cell is considerable weaker in this model than in a higher resolution model with identical physics (Manabe et al., 1979). Seasonally varying insolation is imposed at the top of the atmosphere, and surface temperatures over the ocean and cloudiness are prescribed. Details of the model formulation and the physical processes included can be found in Gordon and Stern (1982) and Manabe et al. (1979), respectively.

We analyze one of the 15-yr integrations of this model examined by Lau (1985). Climatological seasonally varying sea surface temperatures are used everywhere except in the equatorial Pacific (30°S–30°N, 120°E–80°W), where the observed SSTs from the period January 1962 to December 1976 are prescribed. For additional information concerning the GCM calculation, see Lau (1985). We are interested not only in how well idealized barotropic models can simulate the climatology of the upper troposphere in the GCM, but also if such models can be used to study the interannual variability of the GCM's flow.

The GCM's wind field $\mathbf{v}$ interpolated to 200 mb and averaged over 15 summers (June, July, August) is described in Fig. 1 by plots of its (a) absolute vorticity $f + \zeta$, (b) divergence D, (c) streamfunction ψ and (d) velocity potential χ:

$$\zeta = \mathbf{k} \cdot (\nabla \times \mathbf{v}) = \nabla^2 \psi; \quad D = \nabla \cdot \mathbf{v} = \nabla^2 \chi.$$

Also included in Fig. 1e is the corresponding climatological precipitation field. The Tibetan high creates a small region of closed contours in the absolute vorticity field, while the closed contour region in the streamfunction is much larger. The same is true for the model's Mexican high. Stretching, advection of vorticity by the divergent flow, and mixing by transients must combine to produce this striking difference between the vorticity and streamfunction fields. The climatological oceanic upper-tropospheric lows are not as well developed as their climatological counterparts and do not make a dramatic impact on the mean absolute vorticity field. However, these lows are often much better developed in individual months of the integration. The divergence pattern reflects the strong extended maximum in precipitation over East Asia and the western equatorial Pacific, and weaker local maxima over Central America and Africa. Sharp peaks in the divergence tend to be partly compensated by nearby peaks in convergence, as over Central America. Some of the small-scale structure in the divergence near the Tibetan plateau is presumably orographically induced. The velocity potential has a simple structure, mostly represented by zonal wavenumber one, with minimum values to the northeast of the Philippines. The longitudinal variations of the streamfunction and velocity potential are approximately in quadrature on the largest scales.

Consider now the following time–mean vorticity equation in pressure coordinates:

$$0 = \underset{\text{(a)}}{-\mathbf{v}_\psi \cdot \nabla(f+\zeta)} \underset{\text{(b)}}{-\mathbf{v}_\chi \cdot \nabla(f+\zeta)} \underset{\text{(c)}}{-(f+\zeta)D} \underset{\text{(d)}}{+F}, \quad (1)$$

where $\mathbf{v}_\psi$ is the rotational part of the horizontal velocity, $\mathbf{v}_\chi$ is the divergent part, and the variables all refer to the climatological mean. Vertical advection, twisting, transients and the biharmonic diffusion of the GCM are all included in F. Each term of (1) was computed using the GCM's climatological summertime winds interpolated to 200 mb. Unlike Sardeshmukh and Held (1984; hereafter referred to as SH), we are not particularly concerned with obtaining the model's exact vorticity budget; truncation errors in moving from σ-coordinates to p-coordinates should be thought of as included in F. All horizontal derivatives are computed exactly as in the GCM, however.

Plots of the terms (a)–(d) (not shown) are dominated by small scales, and the planetary-scale patterns are difficult to discern. On these scales the stretching is balanced predominately by horizontal advection of relative vorticity, as in SH. However, the term (d), computed as a residual, is not negligible locally, partly due to the neglected terms and partly due to the vertical interpolation. To suppress the small scales, we consider instead the streamfunction budget, obtained by operating with the inverse of the Laplacian on each term in (1):

$$(a)' \equiv \nabla^{-2}(a) = -\nabla^{-2}[\mathbf{v}_\psi \cdot \nabla(f+\zeta)], \text{ etc.} \quad (2)$$

The terms (a')–(d') are shown in Fig. 2, with the zonal mean removed and with the contour interval for (d') one-fifth of that in (a')–(c'). The excellent cancellation on large scales between advection, (a') and (b'), and stretching, (c'), is evident from the smallness of (d'). Note also the importance of advection by the divergent component of the flow (b') on planetary scales in the tropics and the Southern Hemisphere. This term is ignored in the diagnostic model of Holton and Colton (1972) but retained in primitive equation or shallow water models such as those of Webster (1981), Kang (1984) and Gill (1980).

The residual term is a factor of five smaller than the other terms in Fig. 2. We have confirmed that this term is dominated by the contribution from transients, rather than twisting, vertical advection, or ∇^4 diffusion. The contribution of the transients in isolation can be computed by substituting the climatological fields into the GCM's full (σ-coordinate) vorticity equation, operating with ∇^{-2}, and then interpolating to 200 mb. The result is shown in Fig. 3a and is seen to closely resemble the residual (d').

To a first approximation, the transient forcing is out of phase with the eddy streamfunction (see Fig. 8a be-

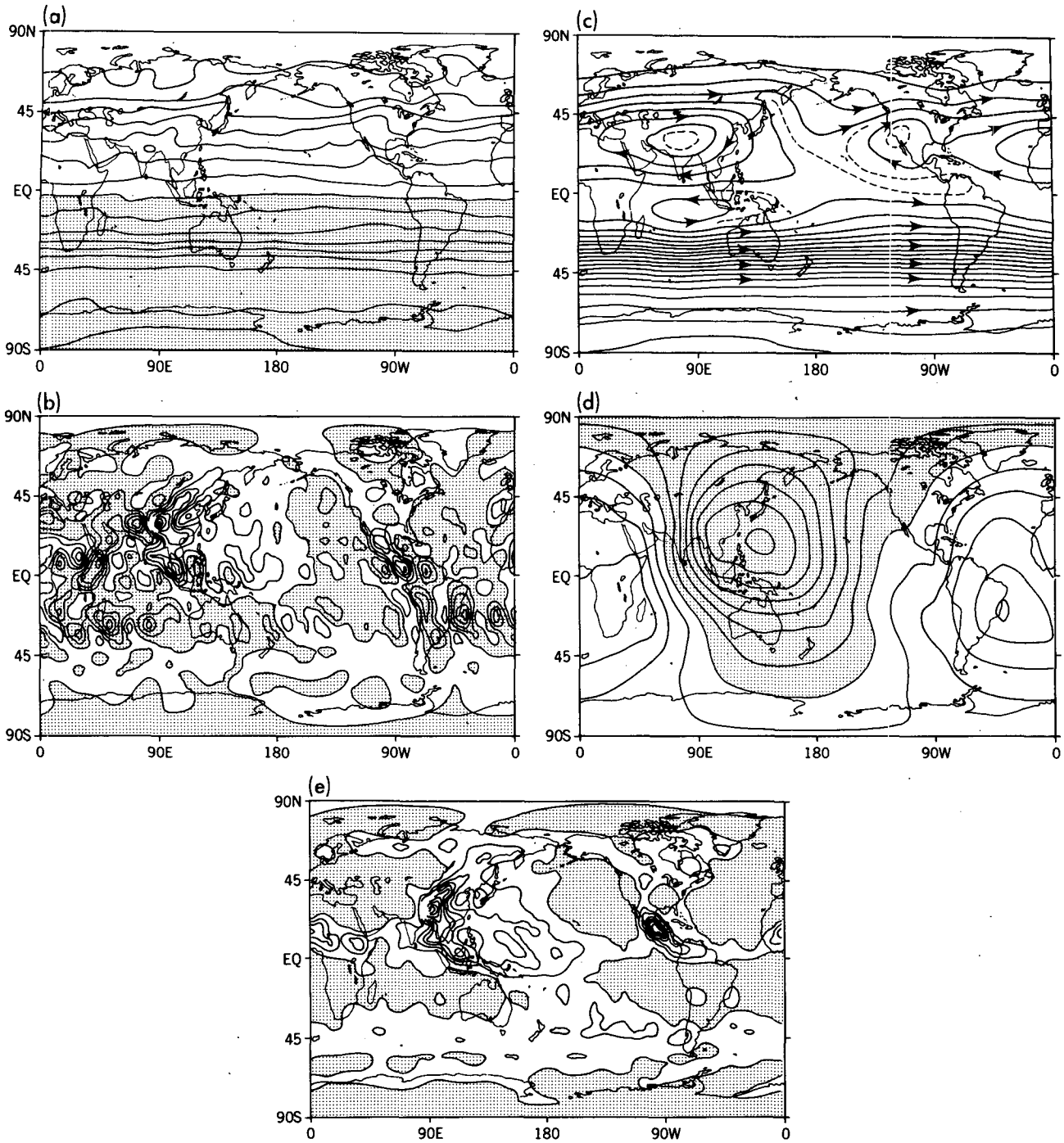

FIG. 1. GCM summertime climatology at 200 mb. Shown are (a) absolute vorticity (2×10^{-5} s^{-1}), (b) divergence (10^{-6} s^{-1}), (c) streamfunction (10^7 m^2 s^{-1}), (d) velocity potential (2×10^6 m^2 s^{-1}) and (e) precipitation rate (2 mm day^{-1}). Contour intervals are indicated in parentheses. Negative values are shaded, except in (e), where shading indicates a precipitation rate less than 2 mm day^{-1}.

low). The implication is that linear damping, $-\kappa\zeta$, might be a useful approximation to this term. Although $\kappa^{-1} \approx 4$ days over the Tibetan region, a more representative value averaged over the tropics is 10 days. To examine the extent to which the damping by transients is scale selective, the effective damping rate κ_l is computed as a function of total spherical wavenumber l:

$$\kappa_l = \mathrm{Re}(\sum \tilde{\zeta}_{lm}{}^* \tilde{F}_{lm})/(\sum |\tilde{\zeta}_{lm}|^2), \qquad (3)$$

where the tilde denotes the complex amplitude of a

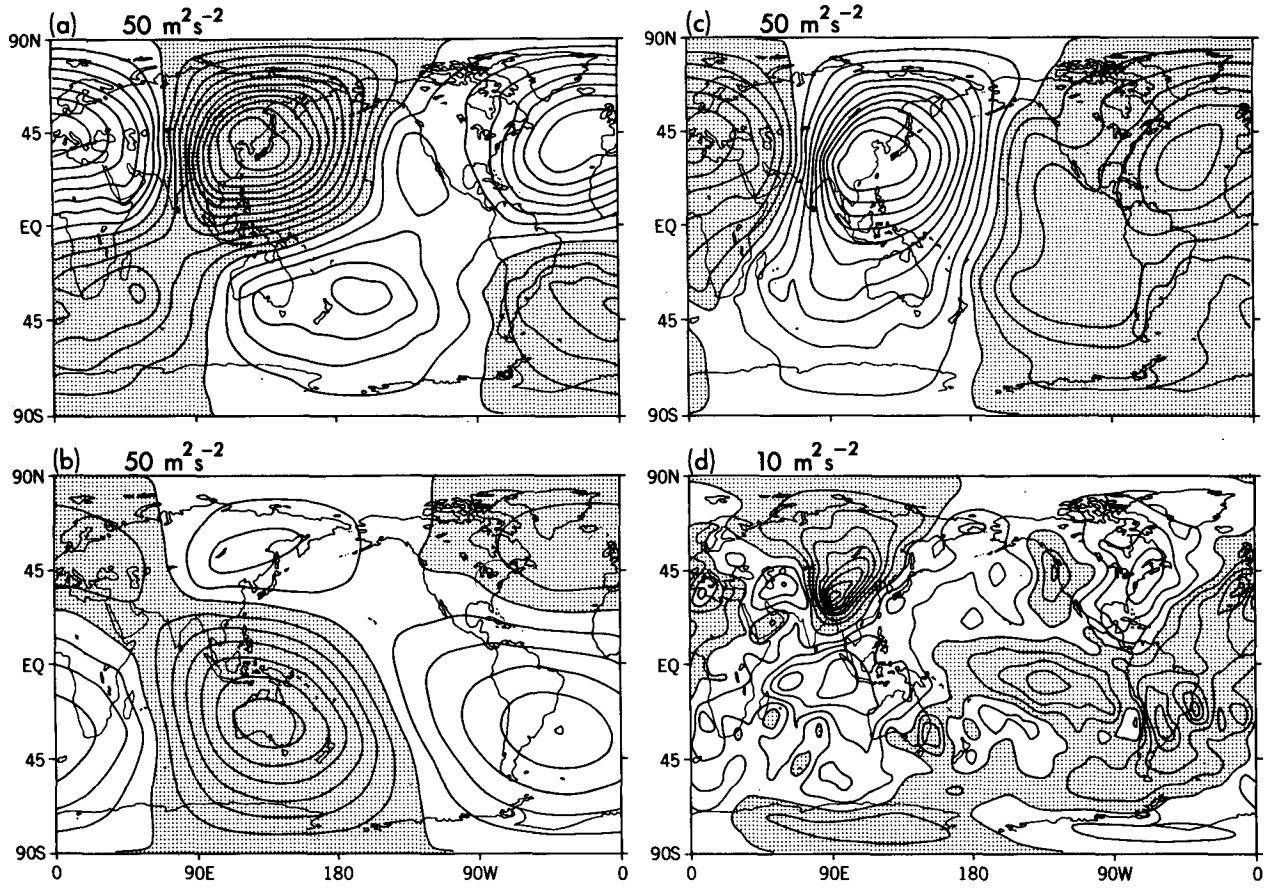

FIG. 2. Streamfunction budget computed using GCM summertime climatology. (a) $-\nabla^{-2}[\mathbf{v}_\psi \cdot \nabla(f+\zeta)]$, (b) $-\nabla^{-2}[\mathbf{v}_\chi \cdot \nabla(f+\zeta)]$, (c) $-\nabla^{-2}[(f+\zeta)D]$ and (d) $\nabla^{-2}F$. Contour intervals are indicated at the top of each panel. Negative values are shaded.

spherical harmonic, the asterisk denotes the complex conjugate, and the sum is over the azimuthal wavenumber m. The resulting damping rate, shown in Fig. 4, shows that small scales generally require a larger damping than large scales; however, the damping appears to be less scale selective than a ∇^2 diffusion, for which $\kappa_l \propto l(l+1)$. For the scales that dominate the eddy streamfunction, l is near 5, and therefore, the appropriate linear damping coefficient might have a value of 1–1.5 ($\times 10^{-6}$ s^{-1}).

We can further divide terms (a′)–(c′) into a part that is linear in the deviation from the zonal mean and a part that is quadratic. Plotted in Fig. 3b is the total contribution to the streamfunction tendency due to the quadratic nonlinearities

$$-\nabla^{-2}[\nabla \cdot (\mathbf{v}'\zeta')]'. \tag{4}$$

A prime refers throughout to the deviation from the zonal mean. The contour interval is again one-fifth of that in Figs. 2a–2c. This term is relatively small over most of the globe, but is comparable in magnitude to the transience in the vicinity of the Tibetan anticyclone. Therefore, the advection terms (a′) and (b′), when linearized about the zonal mean state, yield streamfunction tendencies that are very similar to those in Figs. 2a and 2b. Indeed, both terms are dominated by the effects of planetary vorticity advection, βv. There is Sverdrup balance on the largest scales in the sense that $\nabla^{-2}(\beta v') \approx \nabla^{-2}(fD')$.

We now examine the anomaly (deviation from the summer climatology) in the streamfunction budget produced by the GCM for a particular summer, that of 1966; over the equatorial Pacific, the SST anomalies are mostly positive during the summer following the El Niño of 1965. Figures 5a, 5b and 5c, respectively, show the anomalous eddy streamfunction, stretching (as in Fig. 2c), and residual (as in Fig. 2d), once again with the zonal mean removed. The anomalous residual is taken as an approximation to the anomalous forcing by transients. The anomalous streamfunction is mainly confined to the tropics and subtropics, particularly in the Northern Hemisphere. Waves emanating from the tropics and propagating through great circle paths, which are clearly observed during El Niño winters in the GCM (Lau, 1985), are not obvious, although there is some indication of such a wavetrain in the Southern

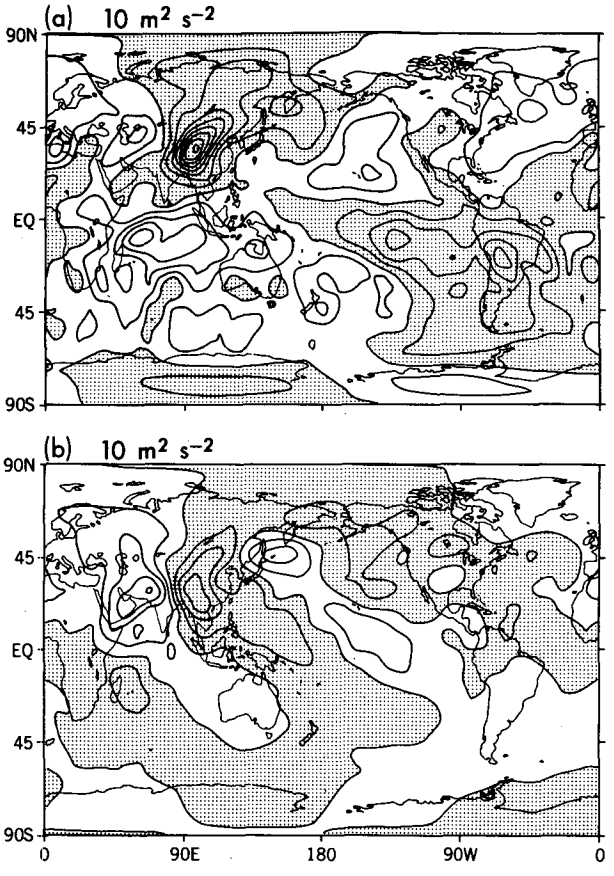

FIG. 3. Nonlinear contributions to GCM 200 mb streamfunction tendency: (a) total transient term and (b) stationary nonlinear term. See text for definitions. Contour interval is shown at the top of each panel.

Hemisphere east of the dateline. The tropical pattern is dominated by a pair of anticyclones about the equator in the Pacific and by a pair of cyclones over the Indian Ocean and southern Asia. Broadly similar anomalous circulations are found in other summers with warm Pacific SSTs and with opposite phase when the tropical Pacific is cold.

As in the climatology, the anomalous stretching is approximately in quadrature with the anomalous streamfunction, indicating that planetary vorticity advection by the anomalous meridional wind balances the changes in stretching on the largest scales. However, comparison of the anomalies in the residual and stretching with their climatological counterparts indicates that the transient forcing is more important for the maintenance of the anomaly circulation than for the climatological flow. (Note that the contour interval for the residual is one-half of that for the stretching in Fig. 5, but one-fifth in Fig. 2.) Also, the tendency due to anomalous transients does not show a clear anticorrelation in space with the anomalous streamfunction, an anticorrelation that is seen in the climatology.

These budget studies provide some guidance in constructing idealized tropical flow models. They confirm that linear models may be valuable on the largest scales, as implied by standard scaling arguments (e.g., Holton, 1979) that one may be able to mimic some of the effect of transients on the climatology with linear damping, and that advection by the divergent component of the flow is important. There is also an indication that simple models of the anomalous streamfunction in a particular summer may run into difficulties because of the anomalous transient forcing. However, it is not straightforward to translate these results into an estimate of the extent to which a particular linear or nonlinear model can simulate the climatological or anomalous stationary-eddy streamfunctions. The analysis in Pierrehumbert and Malguzzi (1984) of an idealized barotropic model serves to remind us that transient mixing can have a major effect on the time mean while having only a minor effect on local vorticity budgets.

3. Nonlinear barotropic models

The prognostic equation for the vorticity that we solve is

$$\partial\zeta'/\partial t = -[\nabla\cdot(f+\zeta)\mathbf{v}]' + F', \tag{5}$$

where $\mathbf{v} = (u, v)$,

$$u = a^{-1}(-\partial_\theta\psi + \cos^{-1}(\theta)\partial_\lambda\chi),$$

$$v = a^{-1}(\cos^{-1}(\theta)\partial_\lambda\psi + \partial_\theta\chi).$$

The velocity potential χ and the zonal mean flow are held fixed at the 200 mb summertime climatological values obtained from the GCM, and only the zonally

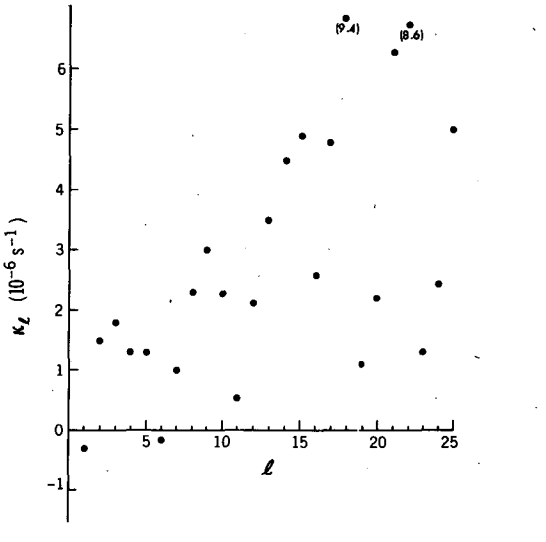

FIG. 4. Effective damping rate κ_l due to the GCM transients as a function of total spherical wavenumber l. See Eq. (3) in text. Two of the points have values off the scale, as indicated.

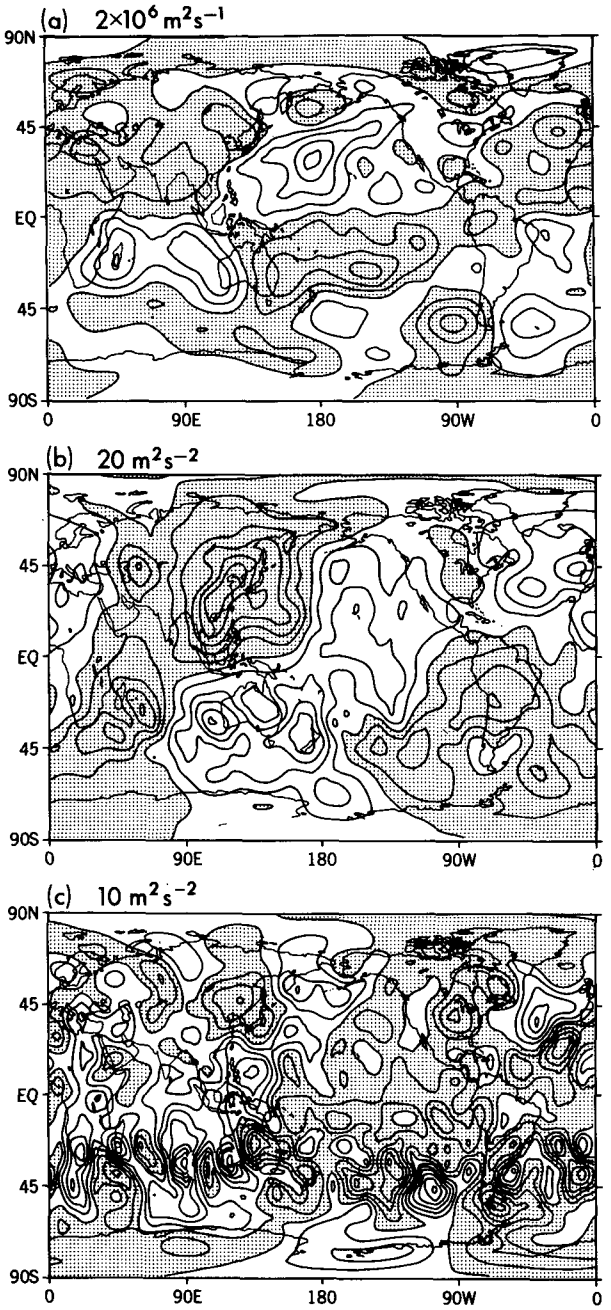

FIG. 5. (a) Anomalous eddy streamfunction, (b) anomalous streamfunction tendency due to stretching, and (c) anomalous residual streamfunction tendency. Anomalies are differences between the 1966 summer mean and the summer climatology. Contour intervals are 2×10^6 m^2 s^{-1} for (a), 20 m^2 s^{-2} for (b), and 10 m^2 s^{-2} for (c).

asymmetric part of the vorticity ζ (or streamfunction ψ) is predicted. Figure 6 shows the prescribed zonal flow; easterlies extend from the equator to 30°N and westerly jets are located near 30°S and 45°N. The term F is the dissipation, and unless otherwise indicated it has the form

$$F = -\kappa\zeta - \epsilon\nabla^4\zeta. \quad (6)$$

The biharmonic diffusion coefficient ϵ is set equal to 10^{16} m^4 s^{-1}, the same value as in the GCM. The linear damping coefficient κ is varied over a wide range. One can think of this linear damping as an attempt to mimic the effects of terms not included in (5), particularly the mixing due to transients that cannot be generated in a barotropic model. The model is integrated with the same spectral method and resolution (rhomboidal truncation at wavenumber 15) as used in the GCM. A 1-h time step is used for all runs, except for one case with $\kappa = 0$ for which we use a 30-min step.

The initial condition is the zonally symmetric climatological flow. The forcing χ is turned on at $t = 0$ and the numerical calculation carried out to 100 days. Depending on the value of κ, the model either asymptotes to a steady state or reaches a statistically steady state with some transient activity. Figure 7 shows the global mean transient kinetic energy averaged from day 50 to day 100 for several values of κ. For κ greater than (15 days)$^{-1}$, the transients are negligibly small, indicating that a stable steady state has essentially been reached. Instability sets in at $\kappa \approx$ (15 days)$^{-1}$, and the transient kinetic energy increases rapidly as κ is reduced further. At $\kappa = 0$, the transient energy is $\approx$60 m^2 s^{-2}, which is roughly one quarter of the transient kinetic energy in the GCM at this level. Further inspection shows that the model transients have a much larger scale than those in the GCM. Whether or not the structure of transients generated in such a model bears any resemblance to the structure of some part (presumably the low frequency part) of the GCM's transients remains to be determined. The critical 15-day damping time is, coincidentally, comparable to the growth rate obtained by Branstator (1985) in his barotropic eigenalysis of the zonally asymmetric (wintertime) climatology of a GCM.

The steady-state eddy streamfunction obtained with κ = (10 days)$^{-1}$ is shown in Fig. 8b. The GCM's climatological eddy streamfunction is shown in Fig. 8a for comparison. The barotropic model is seen to reproduce both amplitude and phase of the streamfunction remarkably well. This result suggests that barotropic models can be of considerable value in trying to understand the tropical upper-tropospheric flow in GCMs and, by implication, in the atmosphere.

Figure 8c shows the eddy streamfunction for the case with $\kappa = 0$ (but with biharmonic diffusion retained to accept the enstrophy cascade) averaged from day 50 to day 100. The time-averaged flow is very similar to the steady flows at much larger values of the drag, despite the presence of strong transient eddies. The same results are obtained with κ = (20 days)$^{-1}$ and (30 days)$^{-1}$. In fact, the time-averaged flows for κ in the range $0 < \kappa <$ (5 days)$^{-1}$ are all quite similar to each other. Although not very evident with the contour interval in Fig. 8, the simulations do distort the Southern

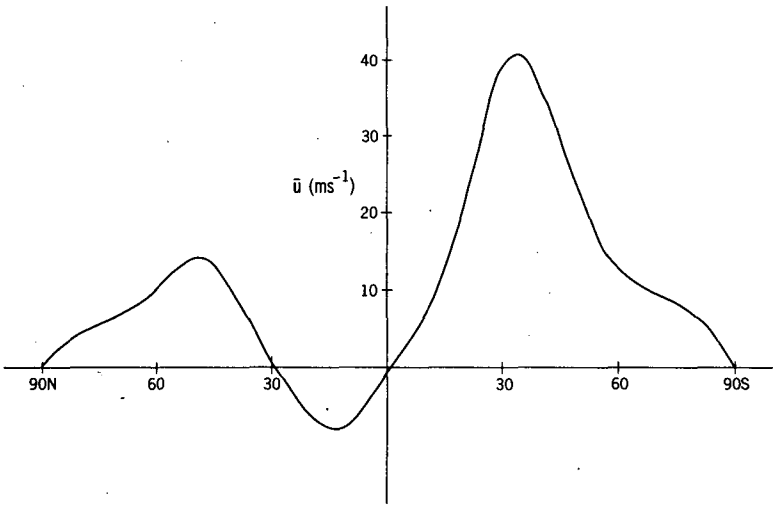

FIG. 6. Zonally averaged 200 mb zonal wind in the GCM summer climatology.

Hemisphere's extratropical streamfunction, most notably off southern Africa when $\kappa = (10 \text{ days})^{-1}$ and over the southern half of South America when $\kappa = 0$. These distortions seem to be due to the generation of anomalously large extratropical wave trains.

Figure 9 shows the streamfunction tendency due to the transients in the $\kappa = 0$ case. The contour interval is 10 $m^2 s^{-2}$ once again. Comparison with Fig. 3a indicates that mechanisms other than barotropic instability are important for generating the transients that contribute to the forcing of the GCM's climatology. The out-of-phase relationship between transient forcing and streamfunction seen in Fig. 3a is not clear here, although there seems to be a tendency toward damping

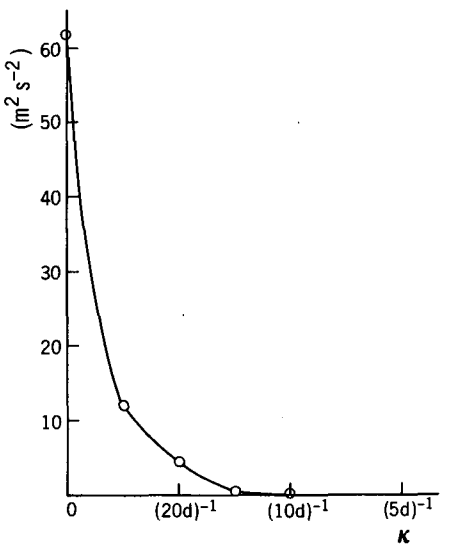

FIG. 7. Global mean transient kinetic energy in the nonlinear barotropic model averaged from day 50 to day 100 for several values of the damping coefficient κ.

near the Tibetan high. The relatively small contribution of the transients to the streamfunction tendency is consistent with the insensitivity of the model solution to a particular choice of the damping coefficient.

Calculations have also been performed with diffusion, $\nu\nabla^2\zeta$, replacing the Rayleigh friction. For $\nu = 1$ or 2 ($\times 10^6$ $m^2 s^{-1}$), the solutions (not shown) approach a steady state and are very similar to those obtained with Rayleigh friction. The insensitivity to the form of the damping mechanism employed is encouraging.

Figure 10 shows the total (zonal plus eddy) absolute vorticity field produced by the nonlinear model with $\kappa = (10 \text{ days})^{-1}$. It is reassuring that the small closed contour region in the Tibetan high (and, therefore, the large difference between the closed contour regions in the streamfunction and vorticity fields) is well simulated.

Having confirmed that the barotropic model can reproduce many aspects of the rotational part of the GCM's flow in the tropics with the divergent part given, one would like to test the possibility of generating the rotational flow from the precipitation field. For this purpose, we have performed calculations similar to those described above, but with D', the zonally asymmetric part of the divergence, set equal to cP', where c is a constant and P' is the zonally asymmetric part of the climatological precipitation field. We choose $c = 4 \times 10^{-6}$ s^{-1}/(cm day^{-1}) based on inspection of Figs. 1c and 1e. This value is consistent with the estimate of Hoskins and Karoly (1981). Since a simple relationship of this sort is not expected to hold in regions where horizontal temperature advection is important, we set $c = 0$ outside of the domain $40°S < \theta < 40°N$. The result obtained with $\kappa = (10 \text{ days})^{-1}$ is shown in Fig. 11. The model still captures much of the structure of the tropical streamfunction, but with less fidelity than the model forced with the GCM's divergence. In particular, the Tibetan high is still more or

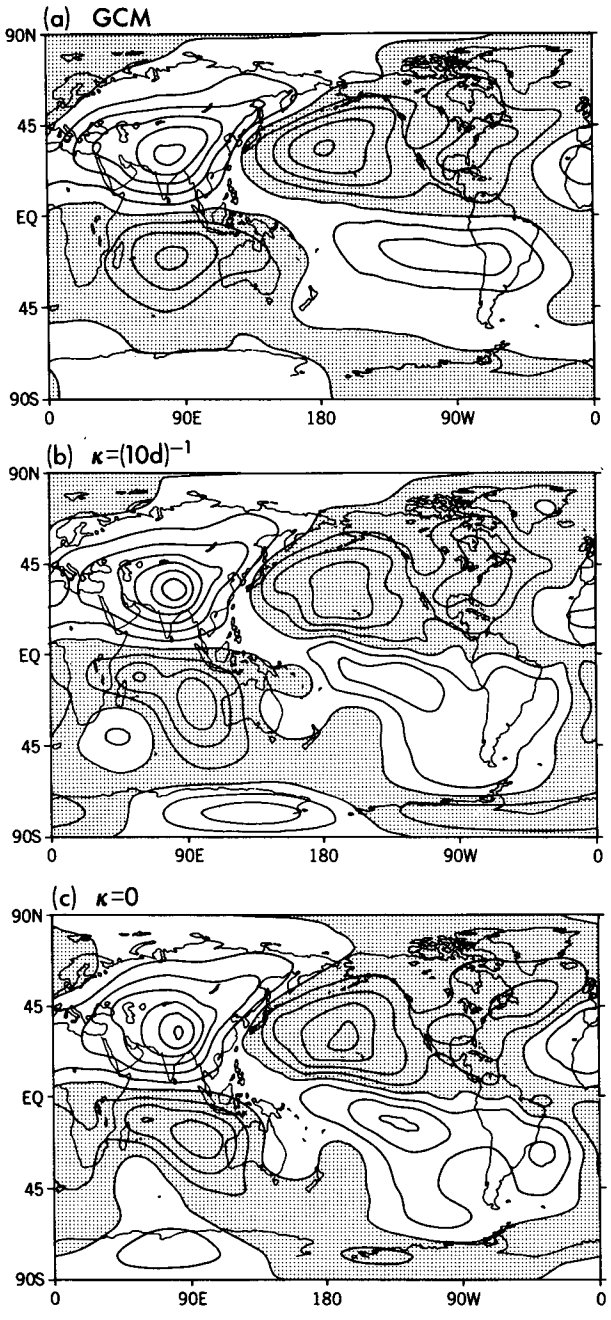

FIG. 8. (a) The GCM's climatological eddy streamfunction during summer. (b) The steady state eddy streamfunction simulated by the nonlinear barotropic model with $\kappa = (10 \text{ days})^{-1}$. (c) The eddy streamfunction averaged from day 50 to day 100 for the case with $\kappa = 0$. Contour interval is $5 \times 10^6 \text{ m}^2 \text{ s}^{-1}$.

less correctly located, although the circulation is too strong. Our choice of c is based on inspection of the regions of active convection, where one expects adiabatic cooling due to upward motion to be closely balanced by latent heating. However, the divergence field also shows regions of localized subsidence near the regions of active convection. These are not apparent in the precipitation field and tend to reduce the amplitude of the resulting planetary-scale rotational flow. One could compensate for this effect by reducing c. In spite of such difficulties, certain features of the GCM's large-scale flow, such as the position of the Tibetan high, can evidently be simulated in a barotropic model by simply setting the divergence proportional to the precipitation rate.

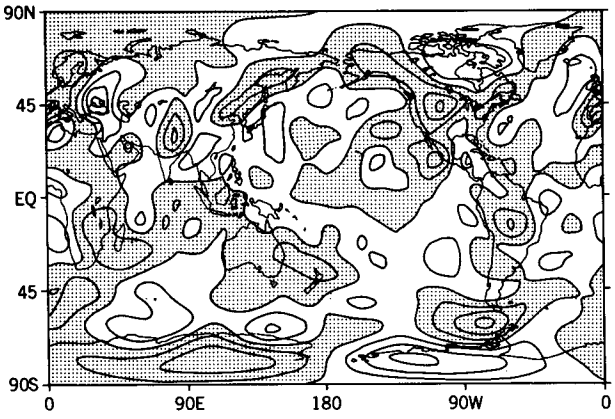

FIG. 9. Streamfunction tendency due to transients in the nonlinear barotropic model with $\kappa = 0$. Contour interval is $10 \text{ m}^2 \text{ s}^{-2}$.

We have also examined the extent to which this nonlinear barotropic model is able to simulate the anomalous flow of a particular summer in the GCM integration. Figure 12 shows $\psi' - \psi_c$, where ψ' is the eddy streamfunction predicted by the nonlinear model given the zonal mean flow and divergence from the GCM's integration for the summer of 1966, and ψ_c is that predicted using the GCM's climatological summertime zonal mean flow and divergence. In Fig. 12a, $\kappa = (10 \text{ days})^{-1}$; in Fig. 12b, $\kappa = (3 \text{ days})^{-1}$. Comparison should be made with Fig. 5a, the GCM's anomalous

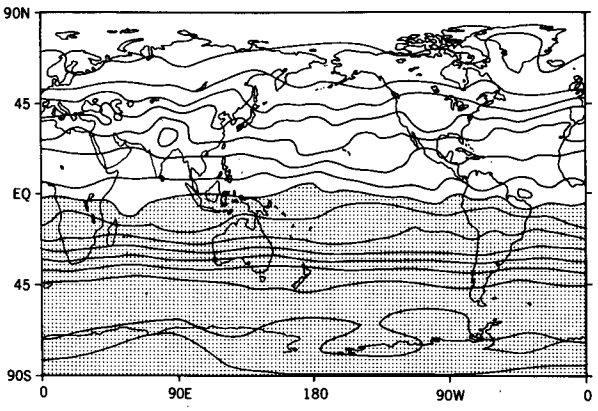

FIG. 10. 50–100 day mean absolute vorticity simulated by the nonlinear barotropic model with $\kappa = 0$. Contour interval is $2 \times 10^{-5} \text{ s}^{-1}$.

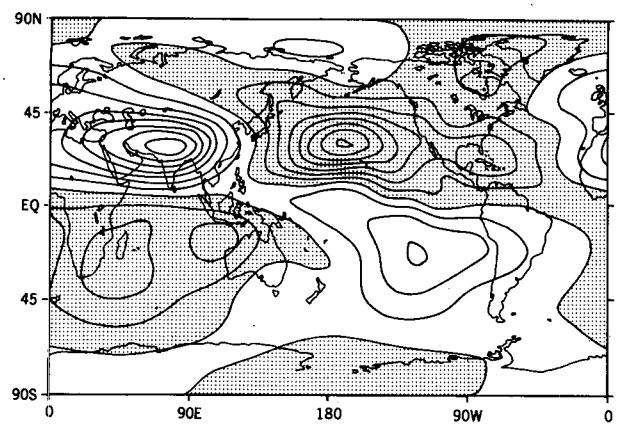

FIG. 11. Eddy streamfunction in the nonlinear barotropic model forced by a divergence proportional to the climatological precipitation rate between 40°S and 40°N. See details in text. Contour interval is 5×10^6 m^2 s^{-1}.

streamfunction in that summer. As shown in the figures, models with small damping predict anomalous streamfunctions that are much too large in extratropical latitudes; however, models with large damping produce qualitatively correct results in the tropics and some extratropical regions. Similar results are obtained when the anomalous GCM circulations for other summers are simulated. Evidently the anomalous transients are important in the maintenance of the anomalous streamfunction, as indicated by the budgets in section 2, and some of the effects of these transients can be crudely mimicked by a strong Rayleigh friction that damps the remote response (despite the fact that the GCM's anomalous transients are not well correlated with the anomalous streamfunction).

4. Linear barotropic models

It is helpful to compare these nonlinear results to the predictions of linear models. Our basic linear model is

$$\partial\zeta'/\partial t = 0 = -\nabla\cdot[\mathbf{v}'(f+\bar{\zeta})] - \nabla\cdot(\bar{\mathbf{v}}\zeta') + F', \quad (7)$$

where $\mathbf{v}' = \mathbf{v}'_\psi + \mathbf{v}'_\chi$, with $\mathbf{v}'_\chi$ prescribed and with F as in (5). Whether or not one includes the zonal mean meridional flow in the basic state makes little difference for the predicted eddy streamfunction; in the following we set $\bar{\mathbf{v}} = (\bar{u}, 0)$. We also consider two simplified versions of this linear model. In the first, we linearize about a state of rest:

$$0 = -\nabla\cdot(f\mathbf{v}') + F' = -\beta(v'_\psi + v'_\chi) - fD' + F'. \quad (8)$$

in the second, we ignore advection by the divergent component of the flow:

$$0 = -[a\cos(\theta)]^{-1}\partial_\lambda(\bar{u}\zeta' + \gamma\varphi') - (f+\bar{\zeta})D' + F', \quad (9)$$

where $\gamma = a^{-1}\partial_\theta(f+\bar{\zeta})$. Equation (8) is the balance assumed in many idealized tropical-flow models (e.g., Gill, 1980). By linearizing about a state of rest in this model, one eliminates the possibility of radiation of stationary Rossby waves away from the region of forcing. In contrast, (9) provides one of the simplest frameworks within which one can discuss the propagation of stationary Rossby waves (e.g., Hoskins and Karoly, 1981).

Figure 13a shows the solution to (7) for $\kappa = (10$ days$)^{-1}$ with climatological forcing. Interestingly, such a weakly damped linear model still bears considerable resemblance to the nonlinear prediction, as well as to the GCM. In particular, the Tibetan anticyclone is located correctly, in contrast to the earlier results obtained by Holton and Colton (1972). But there is too much structure in this anticyclone and in its partner in the Southern Hemisphere as well as in the oceanic low over the Pacific. Inspection of the vorticity field (not shown) shows considerable structure near the zero wind line at 30°N.

The corresponding prediction from (8), Sverdrup balance plus Rayleigh friction, with the same value of κ, is shown in Fig. 13b. As expected, the major differences between Fig. 13a and 13b are in high latitudes in

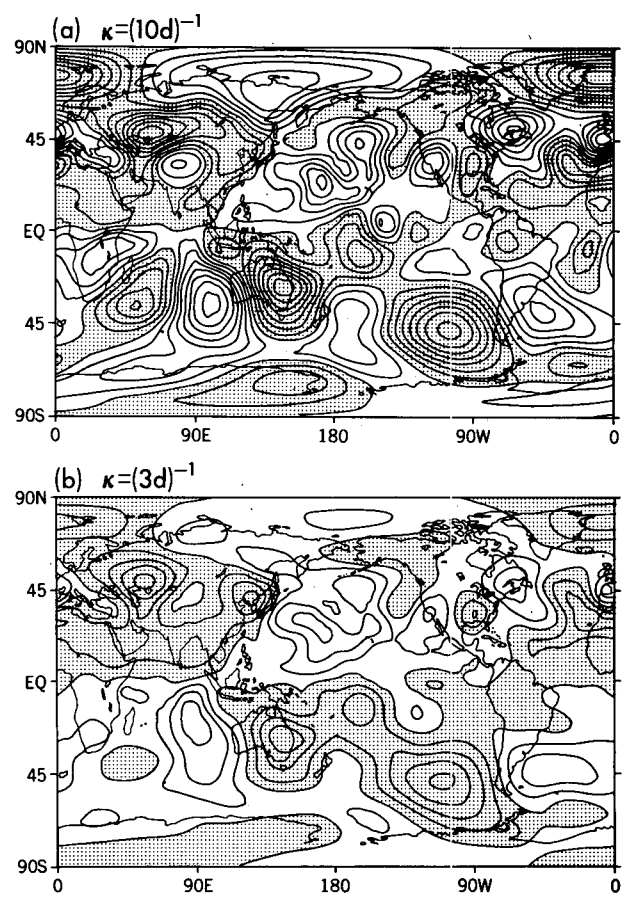

FIG. 12. Anomalous eddy streamfunction for the 1966 summer simulated by the nonlinear barotropic model with (a) $\kappa = (10$ days$)^{-1}$ and (b) $\kappa = (3$ days$)^{-1}$. Contour interval is 2×10^6 m^2 s^{-1}.

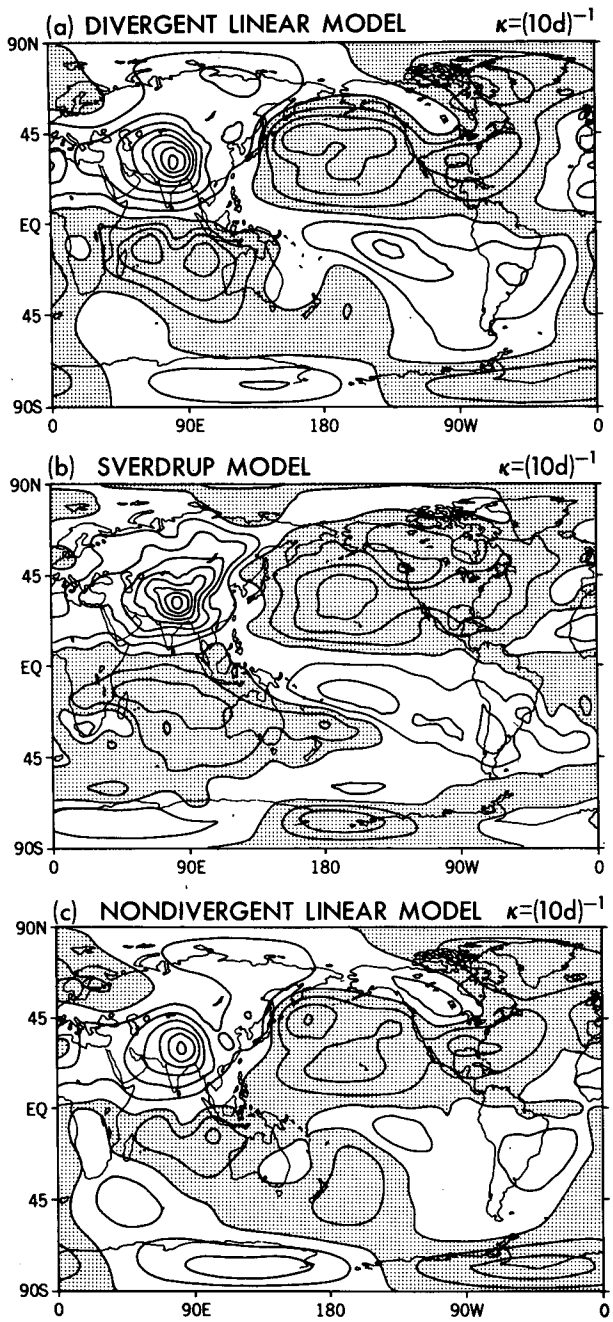

FIG. 13. Eddy streamfunction computed with linear models with $\kappa = (10 \text{ days})^{-1}$: (a) divergent barotropic model, (b) Sverdrup balance model and (c) nondivergent barotropic model. Contour interval is $5 \times 10^6 \text{ m}^2 \text{ s}^{-1}$.

the regions remote from the dominant forcing, while the local responses are similar. Over the Tibetan region, this model also produces too much structure and seems to be too sensitive to the small-scale structure in the divergence in the vicinity of the anticyclone itself, structure that is presumably related to the orography (see Fig. 1). The nonlinear model is less sensitive to this structure, partly because it takes into account the fact that the relatively small absolute vorticity within the anticyclone implies less of a vorticity source or sink for a given divergence.

The prediction of the nondivergent model (9) with the same damping is shown in Fig. 13c. The simulation in midlatitudes is comparable to that in the full linear model, but it has deteriorated significantly in the tropics, particularly south of the equator in the Pacific. Much of the symmetry of the eddy streamfunction about the equator has been lost. The missing ingredient responsible for most of this change is the advection of planetary vorticity by the divergent meridional flow, βv_χ. If one omits this term in the Sverdrup balance model, one finds a similar deterioration of the simulation. In the deep tropics where v_χ is large but f and, therefore, the stretching is small, (8) implies that v_ψ and v_χ tend to cancel each other. This is confirmed by examining the decomposition of the GCM's meridional flow.

Although these linear models are useful, there is little question that the nonlinear model is more robust to changes in the dissipation. Figure 14a shows the so-

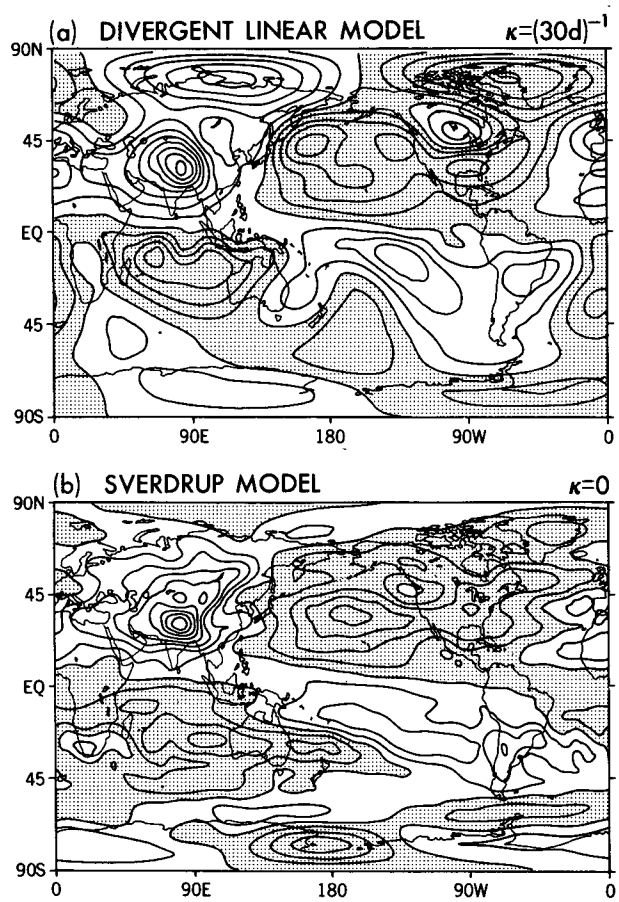

FIG. 14. Eddy streamfunction computed with (a) divergent linear barotropic model with $\kappa = (30 \text{ days})^{-1}$ and (b) Sverdrup balance model without damping. Contour interval is $5 \times 10^6 \text{ m}^2 \text{ s}^{-1}$.

lution to the full linear model (7) with $\kappa = (30 \text{ days})^{-1}$. The local response in the tropics is similar to that in Fig. 13a, but the extratropical response is now unrealistically large. The nonlinear model with small damping (Fig. 8c) provides a far superior extratropical solution for climatological forcing. The manner in which the nonlinearity and transients constrain the amplitudes of the extratropical wavetrains in such a model deserves careful analysis.

For reasons that are not clear to the authors, the weakly damped linear model does not perform as badly here as it does in SH. We suspect that this is due to weaker divergent forcing in the present case, particularly that part of the forcing north of the zero wind line. (We are examining a 15-yr average in a relatively low resolution model; SH consider one month in a model of twice the resolution.) The distortion of the solution around the zero wind line is much greater in SH than here, presumably because much larger Rossby wave trains are generated in their case. In addition, SH do not include biharmonic diffusion in their linear model. If we remove this diffusion in the case shown in Fig. 14a, the response deteriorates further. (Removal of the diffusion in the case with $\kappa = (10 \text{ days})^{-1}$ has little effect.) A linear calculation with $\kappa = 0$ but retaining the diffusion produces an even poorer result, resembling that in SH, in strong contrast to the weakly damped nonlinear model simulation (Fig. 8c).

The importance of local responses for the summer stationary waves in this GCM is well illustrated by Fig. 14b, which shows the solution of the Sverdrup balance model without damping. It is only in the summertime that we find this simplest linear model to have any value. Similar calculations for the winter show no resemblance to the GCM eddy streamfunction.

5. Cumulus friction

While the GCM we are simulating with these barotropic models does not include any vertical transport of momentum in its cumulus parameterization, it is nevertheless of interest to examine how such transport might effect the barotropic model solutions. As a first approximation it seems reasonable to set the upper tropospheric drag due to convection proportional to the precipitation rate and to the upper tropospheric momentum, $\partial \mathbf{v}/\partial t = -\alpha P \mathbf{v}$. Here P is the precipitation rate and α is a constant. Our modified nonlinear barotropic model now reads

$$\partial\zeta/\partial t = -(a\cos(\theta))^{-1}\partial_\lambda\{(f+\zeta)u + \alpha P v\} - (a\cos(\theta))^{-1}\partial_\theta\{\cos(\theta)[(f+\zeta)v - \alpha P u]\} + F, \quad (10)$$

where F now includes only biharmonic diffusion. The divergent part of the flow is once again prescribed. The precipitation field is given its climatological value in the GCM, as plotted in Fig. 1. The value of α, 0.5 cm^{-1}, has been chosen as broadly consistent with the results of Sui and Yanai (1986), who show the cumulus-induced zonal acceleration and precipitation rate during the GATE period. We are assuming that a precipitation rate of 2 cm day^{-1} damps the upper tropospheric momentum with an e-folding time of 1 day.

The time-averaged solution of the barotropic model with this cumulus friction is shown in Fig. 15a. Given the insensitivity of the results of this model to the value of the Rayleigh friction, it is not surprising that this figure is similar to that of the streamfunction obtained without cumulus friction. An exception is the circulation near the Mexican high. In fact, the Mexican high is not very well simulated in the GCM climatological flow, but it is dangerous to take this as proof of the importance of cumulus friction over this region, given the low resolution of the model. Note also that there is very little reduction in the phase shift between the extrema in the streamfunction and velocity potential over East Asia.

The global streamfunction tendency due to cumulus friction is shown in Fig. 15b. It is clearly anticorrelated with the eddy streamfunction, yielding a damping time scale of 5 days over the Northern Hemisphere tropics.

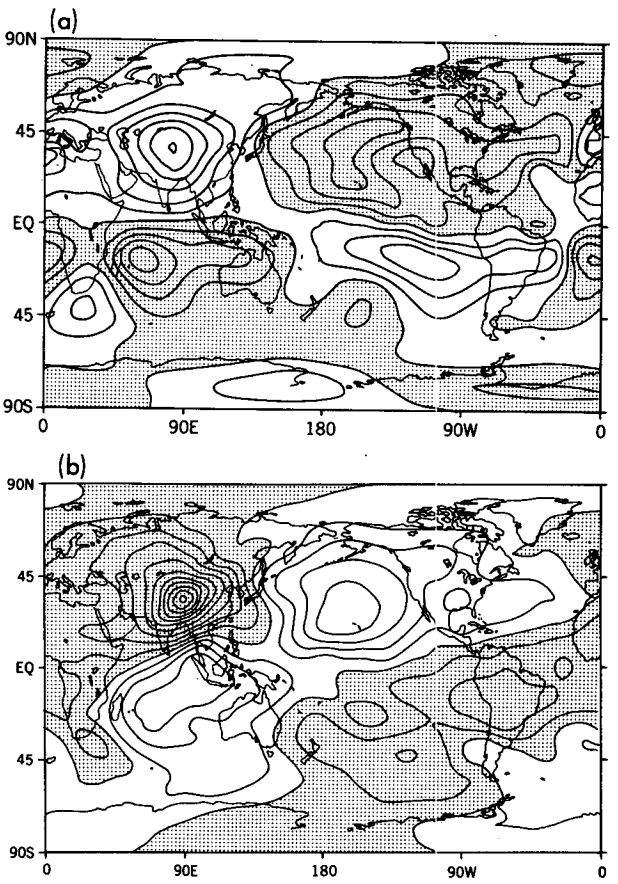

FIG. 15. (a) 50–100 day mean eddy streamfunction simulated by the nonlinear barotropic model with the cumulus friction described in the text. (b) Streamfunction tendency due to the cumulus friction. Contour interval is 5×10^6 m^2 s^{-1} for (a) and 10 m^2 s^{-2} for (b).

Although significant, this damping is still small compared with the terms in the predominant Sverdrup balance shown in Fig. 2, suggesting that cumulus friction is not a major factor in the eddy streamfunction budget during northern summer. However, we have implicitly assumed that the precipitation and, therefore, the upper-tropospheric divergence field remain unchanged when cumulus friction is added to the model. To the extent that these do change, this conclusion would have to be modified. While cumulus friction does not appear to be a dominant term for the planetary-scale stationary waves, it is more likely to be important on synoptic scales, as suggested by many authors (e.g., Yanai et al., 1982; Tollerud and Esbensen, 1984).

6. Concluding remarks

Barotropic models in which the divergence and the zonally averaged zonal flow are specified have been found capable of simulating the climatological eddy streamfunction in Northern Hemisphere summer produced by a GCM. The results are rather insensitive to the strength or the functional form of the frictional parameterization. Even a nearly inviscid model, in which the only friction is the biharmonic diffusion used in the GCM, yields a time-averaged streamfunction that closely resembles that of the GCM. Calculations in which the tropical divergence is taken to be proportional to the precipitation rate confirm that much of the structure in the divergence field that is relevant for forcing the streamfunction is already present in the precipitation field. The barotropic models further suggest that inclusion of cumulus friction in the GCM would not have a dramatic effect on the climatological eddy streamfunction if the large-scale precipitation pattern is not altered significantly.

For this GCM, at least, the simplest Sverdrup balance provides a useful prediction for the position of the Tibetan high. Nonlinearity modifies its structure and strength, but has little effect on its location.

Our discussion of these numerical experiments has been primarily descriptive, in that we have not attempted to explain in detail the interplay between transients and nonlinearity in the GCM or in the barotropic models. The complexity of the divergence forcing in the barotropic simulations is somewhat forbidding. Our impression is that the analysis of barotropic models with more idealized forcing, coupled with idealized GCM integrations, will be needed for this purpose. One of the key questions concerns the amplitudes of the extratropical wave trains generated by tropical heating. While the weakly damped nonlinear model produces much smaller and more realistic climatological amplitudes than weakly damped linear models that allow wave propagation, the anomalous wave trains in individual summers are still grossly overestimated.

Acknowledgments. The authors would like to thank Dr. N.-C. Lau for providing the GCM data used in this study. We also thank Drs. S. Manabe and N.-C. Lau for reading the manuscript and making many constructive suggestions, Dr. S. K. Esbensen for a helpful discussion of cumulus friction, and the members of the Scientific Illustration Group at GFDL for drafting the figures. In-Sik Kang was supported by NOAA/Princeton University under Grant NA84-EAD00057.

REFERENCES

Branstator, G., 1985: Analysis of general circulation model sea surface temperature anomaly simulations using a linear model. II: Eigenalysis. *J. Atmos. Sci.*, **42**, 2242–2254.

Chang, C.-P., 1977: Some theoretical problems of the planetary scale monsoons. *Pure Appl. Geophys.*, **115**, 1087–1109.

Gill, A. E., 1980: Some simple solutions for heat induced tropical circulation. *Quart. J. Roy. Meteor. Soc.*, **106**, 447–462.

Gordon, C. T., and W. F. Stern, 1982: A description of the GFDL global spectral model. *Mon. Wea. Rev.*, **110**, 625–644.

Held, I. M., R. L. Panetta and R. T. Pierrehumbert, 1985: Stationary external Rossby waves in vertical shear. *J. Atmos. Sci.*, **42**, 865–883.

Holton, J. R., 1979: *An Introduction to Dynamical Meteorology.* 2nd ed., Academic Press, 391 pp.

——, and D. E. Colton, 1972: A diagnostic study of the vorticity balance at 200 mb in the tropics during northern summer. *J. Atmos. Sci.*, **29**, 1124–1128.

Hoskins, B. J., and D. J. Karoly, 1981: The steady linear response of a spherical atmosphere to thermal and orographic forcing. *J. Atmos. Sci.*, **38**, 1179–1196.

Kang, I.-S., 1984: Quasi-stationary atmospheric responses to large-scale forcing. Ph.D. thesis, Oregon State University, 140 pp.

Lau, N.-C., 1985: Modeling the seasonal dependence of the atmospheric response to observed El Niños in 1962–76. *Mon. Wea. Rev.*, **113**, 1970–1996.

Manabe, S., D. G. Hahn and J. L. Holloway, Jr., 1979: Climate simulations with GFDL spectral models of the atmosphere: Effects of spectral truncation. GARP Publ. Ser. No. 22, Vol. 1, 44–49. [NTIS N802717.]

Pierrehumbert, R. T., and P. Malguzzi, 1984: Forced coherent structures and local multiple equilibria in a barotropic atmosphere. *J. Atmos. Sci.*, **41**, 246–257.

Sardeshmukh, P. D., and I. M. Held, 1984: The vorticity balance in the tropical upper troposphere of a general circulation model. *J. Atmos. Sci.*, **41**, 768–778.

——, and B. J. Hoskins, 1985: Vorticity balances in the tropics during the 1982–1983 El Niño–Southern Oscillation event. *Quart. J. Roy. Meteor. Soc.*, **111**, 261–278.

Schneider, E. K., 1977: Axially symmetric steady-state models of the basic state for instability and climate studies. Part II: Nonlinear calculations. *J. Atmos. Sci.*, **34**, 280–296.

——, and R. S. Lindzen, 1977: Axially symmetric steady-state models of the basic state for instability and climate studies. Part I: Linearized calculations. *J. Atmos. Sci.*, **34**, 263–279.

Simmons, A. J., J. M. Wallace and G. Branstator, 1983: Barotropic wave propagation and instability, and atmospheric teleconnection patterns. *J. Atmos. Sci.*, **40**, 1363–1392.

Sui, C.-H., and M. Yanai, 1986: Cumulus ensemble effects on the large-scale vorticity and momentum fields of GATE. Part I: Observational evidence. *J. Atmos. Sci.*, **43**, 1618–1642.

Tollerud, E. I., and S. K. Esbensen, 1984: A note on the production of vorticity by parameterized cumulus clouds in general circulation models. Rep. No. 59, Climate Research Institute, Oregon State University, 34 pp.

Webster, P. J., 1981: Mechanisms determining the atmospheric response to sea surface temperature anomalies. *J. Atmos. Sci.*, **38**, 554–570.

Yanai, M., C.-H. Sui and J.-H. Chu, 1982: Effects of cumulus convection on the vorticity field in the tropics. Part II: Interpretation. *J. Meteor. Soc. Japan*, **60**, 411–424.